Application of density functional theory to CO tolerance in fuel cells: a brief review

2009 J. Phys.: Condens. Matter 21 474226

(http://iopscience.iop.org/0953-8984/21/47/474226)

IOP PUBLISHING JOURNAL OF PHYSICS: CONDENSED MATTER

J. Phys.: Condens. Matter **21** (2009) 474226 (9pp) doi:10.1088/0953-8984/21/47/474226

Application of density functional theory to CO tolerance in fuel cells: a brief review

Sergey Stolbov, Marisol Alcantara Ortigoza and Talat S Rahman

Department of Physics, University of Central Florida, Orlando, FL 32816-2385, USA

Received 29 June 2009, in final form 1 September 2009
Published 5 November 2009
Online at stacks.iop.org/JPhysCM/21/474226

Abstract

The large scale practical application of fuel cells in the hydrogen economy is possible only with a dramatic reduction of the cost and significant improvement of the electrocatalytic properties of the electrodes. This can be achieved through rational design of new materials, which requires an understanding of the microscopic mechanisms underlying electrocatalysis. We review briefly some applications of density functional theory (DFT) to this problem, with particular reference to the observed high CO tolerance of Pt–Ru-based anodes. These DFT-based calculations trace the changes in the surface electronic structure and the energy landscape induced by formation of Pt islets on facets of Ru nanoparticles which lead to the preferred diffusion of CO from Pt sites to Ru, where it exhibits a high rate of reaction with hydroxyls, which are generally present. We also consider the energetics of stabilization of the Pt islets on the Ru nanoparticles.

(Some figures in this article are in colour only in the electronic version)

1. Introduction

Fuel cells, invented more than 150 years ago, are currently of great interest, because they are a key element in the emerging energy economy. One of the most promising types is the proton exchange membrane fuel cell (PEMFC), because it can be used for powering transportation vehicles [1]. In PEMFC, protons released in the course of hydrogen oxidation at the anode move through a solid polymer electrolyte membrane to the cathode. At the cathode, the protons meet supplied oxygen and electrons transferred from the anode through the circuit, resulting in an electrocatalytic oxygen reduction reaction (ORR), with water as the final product. PEMFC is a clean source of electric power with low operating temperature (60–80 °C) and high power density. In the direct methanol fuel cell (DMFC), in contrast, hydrogen is supplied not from a separate source but from methanol on the same anode that is used for its oxidation. Though this device provides power with a lower density than PEMFC, it carries the advantage that its fuel, liquid methanol, is easy to store. DMFC can be used as the electric power source for smaller devices, such as cell phones, laptops and cameras.

Although both types of fuel cell thus offer great advantages for various applications, a number of severe obstacles remain to their large scale implementation. To begin with, they are still unacceptably expensive. To make them economically competitive with conventional technologies, their cost has to be lowered by a factor of 10 [1]. Since the Pt-based catalysts currently used in both electrodes of both types of fuel cell make up a major part of the cost, the discovery of new electrocatalytic materials with reduced loading of precious metals is critical for commercialization of PEMFC and DMFC.

There are, moreover, significant shortcomings in the functionalities of these Pt electrocatalysts. PEMFC usually operates with hydrogen obtained from hydrocarbons, which inevitably contain carbon monoxide. Even small traces of CO remaining in the gas after purification poison the Pt anode by blocking its active sites, thereby suppressing hydrogen oxidation [2]. In DMFC, CO released in methanol oxidation supposedly oxidizes with OH obtained from admixed water. Nevertheless, it severely poisons the Pt anode. PEMFC performance suffers even more from a low rate of ORR on the Pt cathode, which results in a high overpotential, and hence low fuel cell efficiency [3]. In DMFC, methanol, undesirably transferred onto the Pt cathode, additionally reduces the ORR rate [4].

Because the large advantages of fuel cells can be efficiently utilized only if the cost of the electrodes is dramatically reduced and their electrocatalytic properties are significantly improved, enormous effort is being invested to find new materials that meet these requirements. Notable progress has already been made in improving the CO tolerance of the anode. It is known that alloying of Pt with a second (and even third) metal element may reduce the poisoning of Pt sites through CO adsorption. For example, Pt–Ru alloys are

found to be more tolerant to CO than pure Pt [2]. Alloying Pt with Sn [2] and Mo [5] also improves anode performance. These anodes are nevertheless still strongly affected by CO poisoning. Another disadvantage of these materials is still a high loading of expensive platinum. Not surprisingly, the report by Brankovic *et al* that nanoclusters of Ru with a sub-monolayer of Pt ($PtRu_{20}$) are much more tolerant of CO poisoning than commercial PtRu catalysts [6, 7] has thus been welcomed with optimism. It is also important that the content of Pt in this novel material is much lower than that in Pt–Ru alloys. From their estimates of the average diameter of Ru nanoparticles (2.5 nm) and of the Pt/Ru ratio, the authors conclude that the deposited Pt forms small islands (islets) on the facets of the Ru nanoparticles.

Some progress has also been achieved in improving the cathode properties. Apart from reduced Pt loading, some PtM alloys (M = Ti, V, Cr, Mn, Fe, Co and Ni) [8, 9] have been found to demonstrate improved ORR kinetics. Several groups have reported significant progress in reducing Pt loading and increasing reactivity with electrocatalysts consisting of a monolayer of Pt on carbon-supported metal or metal–alloy substrates [10–13]. Compounds and alloys of non-noble metals also exhibit promising electrocatalytic properties for cathode catalysts. Bimetallic $PdCo_x$ [14–17], Ir_xCo_{1-x} [18] and Pd–Cu [19] compounds and alloys are cases in point. Xiao *et al* have recently shown that these Pd nanorods are 10 times more active towards ORR than Pd nanoclusters [20]. Nitrides of the transition metals also appear to be promising non-noble electrocatalysts for oxygen reduction. For example, Zhang *et al* [21] observed ORR with comparatively good performance on carbon-supported molybdenum nitride (γMo_2N) nanoparticles of 4 nm average size. An even higher ORR rate, combined with enhanced methanol tolerance, has been reported recently for the hexagonal MoN [21]. Carbon-supported CrN [22] and $CrC_{0.39}N_{0.61}$ [23] are also found to be catalytically active for oxygen electro-reduction. Interestingly, the size of CrN nanoparticles apparently influences the reactivity of the cathode [22]. Many other nitrides of transition metals are reported to catalyze oxygen electro-reduction. Among these are Fe–N and Co–N [24]; Co–C–N [25] and Fe–C–N [26]; ZrC_xN_y [27]; Ta_3N_5 and TaO_xN_y [28]. Although the ORR rate on these cathodes is still lower than it is on Pt-based ones, the low cost of these nitrides of transition metals and their wide range of elemental composition and geometric structure strongly justify further search for new materials of this family. In general, the reactivity of catalysts is determined by the nature of chemical bonding between the catalyst and reactants or intermediates, which in turn depends on the composition, geometric structure and size of catalyst particles. Nanometer-sized particles are expected to have an increased number of steps at the surface and chemically undersaturated sites (CUS) at the facet edges. This is important, because CUS are naturally more reactive and the steps at metal surfaces are known to dramatically enhance oxygen dissociation [29], one of the key elements of ORR. Further decrease in nanoparticle size may bring into play quantum size effects, which may also substantially affect catalytic properties. Search for efficient catalysts can thus be performed by varying composition and particle size and by modification of the surface structure of the system. Since this involves many variables, the search will be more efficient if there is a prior understanding of the microscopic mechanisms controlling the catalytic processes.

In heterogeneous catalysis these mechanisms essentially depend on the energetics and pathways of the elementary steps such as adsorption, diffusion and reaction of reactants and their intermediates on the catalyst surface. These microscopic quantities can be obtained from first-principles calculations based on density functional theory [30, 31] and then used to estimate the rates of the elementary processes and the rate-limiting steps [32]. Analysis of the electronic charge densities and densities of electronic states calculated for various stages of the reaction may also reveal the factors controlling the reaction energetics and hence serve as a basis for the rational design of new catalysts. Finally, the activation barriers obtained from DFT calculations can be used in kinetic Monte Carlo (KMC) simulations to obtain the temperature and pressure dependences of the total reaction rate [33], thereby enabling a multiscale approach in which microscopic characteristics, obtained within DFT for zero temperature, are used to characterize and potentially predict the mesoscopic kinetic processes at finite temperatures.

The kinetics of electrocatalysis in fuel cells may present a further complication in the form of electron and proton transfer between two electrodes with different Fermi levels. It has been shown, however, that some approaches from conventional heterogeneous catalysis and gas phase reactions can be used to describe the electrocatalytic phenomena [34] by choosing a reference which links gas phase and electrocatalytic quantities. Different choices of this reference have resulted in different models. In order to model electron transfer, Anderson and Albu [35, 36] calculated the free energies of reactants on a cluster with different numbers of electrons. This model, however, is applicable only to small-sized clusters. Further developments in this direction are nicely described in a review article by Shi *et al* [37]. In another approach to the problem, Nørskov *et al* [34] set the reference potential as $\mu(H^+ + e^-) = \mu(\frac{1}{2}H_2)$ so as to allow replacing the energy of the $n(H^+ + e^-)$ transfer with the energy of a hydrogen molecule and a corresponding multiplier. Within this approach they first calculate adsorption energies of reactants and intermediates using a DFT-based method. For adsorption configurations achieved through processes involving electron transfer, relevant bias effects are taken into account by shifting the energy by $-eU$, where U is the electrode potential. A free-energy diagram of these configurations can then be constructed as a function of the electrode potential. Although this method provides extraction only of thermodynamic characteristics, and not system kinetics, it can be very useful for understanding trends in electrocatalytic processes. For example, using this approach Nørskov *et al* [34] have revealed the origin of the overpotential for ORR on the Pt cathode. Further improvement of this method has been developed by Nørskov's group [38] by taking into account the effects of local electric fields in the electric double layer on the free energies of reactants and intermediates. In this approach, an estimated field of an

electric double layer at the electrode was included in the DFT potential. Yet another approach [39] takes into consideration the entire electrode–electrolyte interface within the periodic slab model. The electric field is introduced by changing the number of electrons in the slab and compensating for their charge by distributing a uniform charge over the entire supercell. In this method the work function of the electrode–electrolyte system directly determines the electrochemical potential. Interestingly, these three models give almost the same results for the electrochemical oxidation and reduction of water [40].

In electrocatalysis, some important processes (e.g. O_2 dissociative adsorption on the fuel cell cathode, CO adsorption and diffusion on the anode) do not involve electron or proton transfer, making these processes similar to the elementary ones in conventional heterogeneous catalysis. The only difference is that the reactants experience the electric field caused by the potential difference between the electrodes. This effect has been estimated for the O and OH intermediates adsorbed on Pt using the approach mentioned above [38]. Assuming the dipole moments of adsorbed O and OH to couple with the electric field caused by change in the potential within the 3 Å electrochemical double layer, Nørskov *et al* found the energy of such an interaction to be negligible. Density functional theory—long used as an insightful and reliable theoretical and computational tool in understanding the fundamental steps in heterogeneous catalysis—may thus also be applied to examine reactions in fuel cells that do not involve electron or proton transfer.

In addition to reactivity of an electrocatalyst, its stability is a very important property. The most promising electrocatalysts are inhomogeneous systems, such as the CO tolerant anode with Pt islets on Ru nanoparticle [6, 7]. It is not obvious that these structures will remain stable, particularly in reaction environments. Other promising electrocatalysts—such as Pt–Fe [37] and Pd–Co alloys—undergo segregation, resulting in formation of a 'skin' layer (or layers) of Pt or Pd atoms on the alloy surfaces. Since electrocatalytic activity strongly depends on the composition of the electrode, such transformations may significantly affect the desired properties. It is thus important to understand the relationship between material structure and composition. Some insight into this relation may be obtained using a computational approach based on DFT.

For this special volume dedicated to Richard Palmer, with the above background we present here a short review of an application of DFT-based calculations to unravel the mechanism of CO tolerance of the Pt/Ru nanostructures reported in [6] and to the stability of these nanostructures. The material presented below has been extracted from two recent publications [41].

2. First-principles studies of CO energetics on Pt–Ru nanostructures: rationale for tolerance

Since CO poisons the reactivity of the Pt anode by blocking its active sites, an obvious way to reduce this poisoning is to facilitate the removal of CO from these sites. A number of publications have thus focused on understanding the mechanisms of CO adsorption on Pt–Ru systems [42–44]. For example, Koper *et al* [42] have calculated from first principles the CO adsorption energy E_{ad}(CO) on clean Pt(111) and Ru(0001) surfaces, as well as on a Pt monolayer over Ru(0001) and an Ru monolayer over Pt(111). As E_{ad}(CO) is found to be the lowest for the case of a monolayer of Pt on Ru(0001) (Pt_{ML}/Ru(0001)), Koper *et al* propose this lowering as the explanation for the high CO tolerance of this system. Furthermore, first-principles study of alloying effects on CO adsorption on Pt [43, 44] suggest that strain induced by the second element modifies the electronic states of Pt in such a way as to cause a decrease in CO adsorption energy.

In general, the removal of a CO molecule from the Pt sites can be achieved either by desorption or diffusion. However, in the above-mentioned case of Pt_{ML}/Ru(0001), in which only Pt atoms are exposed to the surface, the only mechanism for CO removal is desorption. The desorption rate R can be estimated using transition state theory:

$$R = D_0 e^{-\frac{\Delta E}{kT}}, \tag{1}$$

where D_0 is the pre-factor and, for this particular process, $\Delta E = E_{ad}$(CO). Setting $D_0 = 10^{12}$ s^{-1}, which is a typical value for the pre-factor, $T = 350$ K (operational temperature for PEMFC), and taking $\Delta E = 1.11$ eV from [17], we obtain $R \approx 10^{-4}$ s^{-1}. The desorption rate is thus very low for Pt_{ML}/Ru(0001) and it is expected to be even lower for other anodes, because of higher E_{ad}(CO).

The observed enhancement of the CO tolerance of the Pt/Ru nanostructure thus cannot be caused by an increase in the desorption rate. Missing from this analysis is the consideration of CO diffusion rates, which for anodes with inhomogeneous surfaces such as the $PtRu_{20}$ nanoparticles [6] may be the main factor contributing to the CO removal from Pt sites. Spillover of CO from Pt islands to the Ru substrate is mentioned in [45] as a possible mechanism for the high CO tolerance, but the argument bases itself on the assumption of weakened CO adsorption. The spillover rate, however, depends on the diffusion of the molecules, which is implicitly related to its adsorption. Conclusions about the efficiency of the CO spillover thus need to be based on knowledge of activation energy barriers for CO diffusion in the system, which can be obtained from accurate DFT calculations. We have performed such calculations for CO diffusion on Pt islands on the Ru(0001) surface to model the presumed dominant facet of the $PtRu_{20}$ nanoparticle [41]. We have calculated the energetics of the system along the entire path of the CO molecule's diffusion from the center of the Pt island to its edge and, further, into the Ru substrate.

2.1. Computational details

Our calculations have been carried out within DFT using the plane wave pseudopotential method [46] as embodied in the code VASP [47] with ultrasoft pseudopotentials [48]. To maintain the periodicity of the systems we used a supercell composed of a five-layer Ru(0001) slab with a four or seven Pt-atom island, on one side, and a vacuum layer of 15 Å. The CO molecule was adsorbed either on the island or on the Ru(0001)

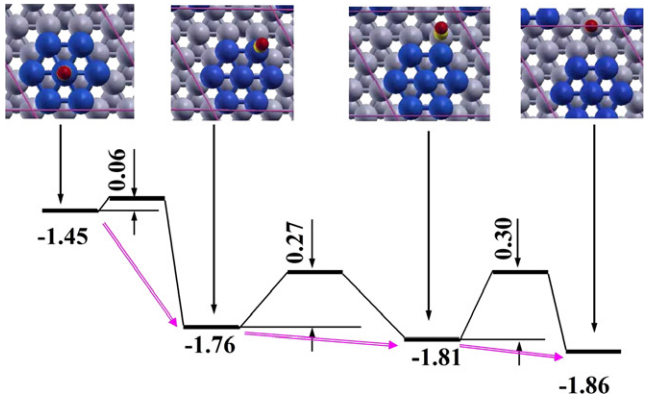

Figure 1. Energetics for CO diffusion from the center of Pt islet (c-Pt site) to its edge (e-Pt) and further to Ru substrate (n-Ru and nn-Ru sites). The dark-small (red in the online version), light-small (yellow in the online version), dark-large (blue in the online version) and light-large (gray in the online version) balls represent O, C, Pt and Ru atoms, respectively. Negative and positive numbers correspond to CO adsorption energies and CO diffusion energy barriers, respectively.

substrate. To diminish interaction between the periodic images of Pt islands, the supercell was extended along the (0001) surface making up the (4 × 4) superstructure. With such a geometry, the shortest distance between edges of neighboring islands equaled two Ru–Ru bond lengths. The supercell contained 80 Ru atoms, plus Pt atoms forming the island and a CO molecule. The Brillouin zones were sampled with (3 × 3 × 1) Monkhorst–Pack k-point meshes [49]. We used a kinetic energy cutoff of 400 eV for the wavefunctions and 700 eV for the charge density in order to ensure sufficient computational accuracy for the oxygen-containing structures. We used the Perdew–Wang generalized gradient approximation (GGA) [50] for the exchange–correlation functional.

To achieve structural relaxation, a self-consistent electronic structure calculation was followed by calculation of the forces acting on each atom. Based on this information, the atomic positions were optimized to obtain equilibrium geometric structures in which forces acting on atoms do not exceed 0.02 eV Å^{-1}. To locate the transition states for the CO diffusion, we obtained the total energies for the relevant pieces of the potential energy surface by fixing in-plane coordinates of the C atom belonging to the CO molecule and letting the system relax for all other degrees of freedom.

2.2. Results and discussion

We present here results for the seven-atom Pt islet on the Ru(0001) surface (7Pt/Ru(0001)). We have calculated the energies of CO adsorption on top of the central (c-Pt) and edge (e-Pt) platinum atoms and on two non-equivalent (fcc and hcp) hollow sites, as well as on the Ru substrate site neighboring the Pt islet (n-Ru) and the next-neighbor Ru site (nn-Ru). In addition, activation energy barriers have been calculated for CO diffusion from c-Pt to e-Pt, between two e-Pt (along the island edge), from e-Pt to n-Ru, and from n-Ru to nn-Ru sites. Figure 1 shows the energetics calculated for the system with CO moving along the c-Pt → e-Pt → n-Ru → nn-Ru path.

As illustrated in figure 1, CO bonding increases as the molecule moves from the center of the Pt island to its edge and further to the Ru(0001) substrate. This negative gradient of E_{ad}(CO) along the c-Pt → e-Pt → n-Ru → nn-Ru path already indicates that the CO molecule adsorbed on 7Pt/Ru(0001) would prefer to leave the islet for the Ru substrate. Furthermore, we find E_{ad}(CO) = −1.94 eV for CO on clean Ru(0001). This value is lower than those for CO adsorption on the n-Ru and nn-Ru sites, suggesting that CO tends not only to leave the Pt islet, but also to move away from it.

The activation energy barrier for CO diffusion from c-Pt to e-Pt through the bridge site is found to be as low as 0.06 eV. The barriers for the rest of the considered path are also quite low. The highest n-Ru–nn-Ru barrier is 0.3 eV, resulting in a diffusion rate $R \approx 5 \times 10^7$ s^{-1} from equation (1) with $D_0 = 10^{12}$ s^{-1} and $T = 350$ K. Clearly, this rate is much higher than that for CO desorption. We thus find the spillover of CO from Pt islets to Ru substrate to be a favorable process, which keeps active Pt sites available for hydrogen oxidation, hence providing the high CO tolerance of the $PtRu_{20}$ nanostructure. Interestingly, we find CO bonding to the Pt island atoms to be significantly stronger than its bonding to Pt_{ML}/Ru(0001) (we obtain E_{ad}(CO) = −1.15 for Pt_{ML}/Ru(0001), which differs slightly from −1.08 eV reported in [6]). For the edge-Pt atom it is even stronger than CO bonding to Pt(111) (−1.6 eV). Nevertheless, this system provides a very efficient mechanism for CO removal from active Pt sites—and this mechanism originates not from weak CO bonding to Pt atoms but from the negative adsorption energy gradient and low energy barriers for CO moving from the center of the Pt island to its edge and on to the Ru(0001) substrate. The calculations have also been performed for a four-atom Pt islet on Ru(0001), in which all Pt atoms belong to its edge. It is thus not surprising that the obtained E_{ad}(CO) = −1.78 eV is almost the same as for the edge-Pt atoms in 7Pt/Ru(0001) (−1.76 eV). We can thus expect the same spillover scenario for smaller islands.

Since we consider here CO adsorption on a Pt-containing system, we have to address the issue Feibelman *et al* [51] call 'the CO/Pt(111) puzzle'. As they noticed, DFT calculations suggest that hcp hollow sites are preferred for CO adsorption on Pt(111), Cu(111) and Rh(111), while experiments indicate that the top sites of these surfaces are preferred. More accurate calculations [52] resulted in the correct (top) site for Rh(111). Grinberg *et al* [53] find the error to originate mostly from the exchange–correlation approximations which overestimate CO binding to the hcp sites, while the top sites' adsorption is treated correctly. Kresse *et al* [54] suggested that such behavior is caused by the underestimated gap between the highest occupied and lowest unoccupied states of CO by DFT. In the present calculations, the CO binding energy is found to be much higher for the top e-Pt site than for the hollow sites, suggesting that for this system 'the puzzle' does not emerge. This may be caused by significant modification of the Pt d-states due to their hybridization with the Ru d-states. Furthermore, the pathway for the CO spillover found in our calculations goes through the top adsorption sites, for which the DFT calculations are expected to be accurate [53].

3. First-principles studies of the energetic of Pt islands on Ru: rationale for stability of nanostructures

The above spillover mechanism of CO removal from the catalytically active Pt sites of the Pt–Ru nanostructures appears to depend critically on the size of the Pt island. This naturally raises the question of stability of a structure with several-atom Pt islands on the Ru substrate, which is related to the problem of the heteroepitaxial growth. Theoretical models of heteroepitaxial growth suggest that the growth mode is determined by a competition of such factors as the surface energies of the bare substrate and the heteroepitaxial layer, the interface free energy and the strain energy introduced by the lattice mismatch of the two species [55, 56]. For example, a mismatch in the respective bulk-lattice constants strains the interface and may set off the 3D clustering growth mode [56]. In contrast, growth of ad-layers with lower surface energy than the substrate's may favor the 2D layer-by-layer growth mode [57]. Considerations along these lines, however, lead to ambiguities in predicting Pt growth on Ru(0001). While the higher cohesive energy of Ru (relative to Pt) may [58, 59] imply that the surface free energy of Ru(0001) is higher than that of Pt(111) and point to 2D layer-by-layer growth, the stress caused by the Ru–Ru and Pt–Pt bond-length misfit (the bond lengths in bulk Ru and Pt are 2.706 Å and 2.775 Å, respectively [60]) may lead to 3D clustering. There may also be competition between the above two factors, leading to a critical Pt island size at which there is crossover between 2D and 3D growth modes or island–substrate atom exchange [56, 61]. One of the goals is thus to determine whether there is indeed a critical size beyond which 2D Pt islands are no longer stable on Ru(0001).

In the experiments in question [5, 6], Ru nanoparticles have well-developed facets divided by edges. Since one of the dominant facets has the Ru(0001) geometry [6], as a first step in the modeling of the Pt–Ru nanoparticles, we consider the formation of Pt islands as a function of size on the Ru(0001) surface. To this end, we carry out first-principles calculations of the system total energy to determine the geometry and formation energy of Pt islands, as well as that of 1 ML of Pt on Ru(0001). Clearly, the main drawback of such calculations is that the predictions are relevant to zero temperature for samples relaxed in infinite time. The kinetics of the system can be partially included by taking into account diffusivity of Pt ad-atoms. At least for low temperatures, the three aforementioned growth modes can be understood in terms of diffusion-barrier differences between one-step hopping and step-descending hopping (Schwoebel barriers) [62–64]. If the Schwoebel barrier is positive, the probability for the ad-atoms to be trapped on the step terraces is high, so that 3D clustering is favored. In contrast, if the Schwoebel barrier is zero or negative, the ad-atoms that happen to lie on the step terrace are more likely to hop onto the substrate, thus favoring 2D growth [63]. To understand the role of such effects in the formation of Pt islands on Ru(0001) we also calculate the barriers for the diffusion of Pt atoms from the eight-atom island to the Ru substrate.

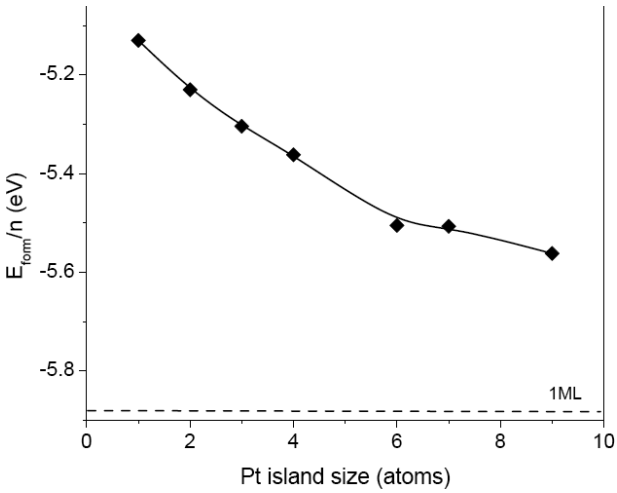

Figure 2. Average formation energy per Pt atom, E_{form}/n, as a function of the size, n, of the Pt island. Dashed horizontal line marks the E_{form}/n value for one Pt monolayer on Ru(0001).

3.1. Pt islands on Ru(0001)

To reveal stable configurations for the sub-monolayer Pt deposited on the Ru(0001) substrate, we have calculated the optimized geometric structure and energetics of the 1 to 9 Pt-atom islands and one Pt monolayer on Ru(0001) using the (4×4) supercell. To characterize the stability of a given Pt island, we obtain its formation energy, defined as

$$E_{\text{form}} = E(\text{Ru} + \text{Pt}) - E(\text{Ru}) - nE(\text{Pt}_{\text{at}}).$$

Here, $E(\text{Ru} + \text{Pt})$ is the total energy of an Ru slab adsorbed with a n-atom Pt island, while $E(\text{Ru})$ and $E(\text{Pt}_{\text{at}})$ denote the total energies of the clean Ru slab and of a free Pt atom, respectively. Note that the formation energy of stable structures should be negative. The structure with lowest average formation energy per Pt atom, E_{form}/n, is thus distinguished as the energetically most favorable one. Figure 2 presents E_{form}/n as a function of the size of the island. Note that the horizontal line at the bottom of the panel marks the formation energy per atom for a Pt monolayer on Ru(0001) which is found to be -5.89 eV. We find that the larger the Pt island, the higher its stability is. Such a trend culminates and is confirmed at full monolayer Pt coverage, which provides lowest E_{form}/n.

We also explored the effect of the Pt atom detachment from islands. Figure 3 shows two configurations considered for the seven-atom Pt island adsorbed on Ru(0001). We find the detachment (transition from the left to the right configuration in the figure) to cause an increase in E_{form} from -38.55 to-37.52 eV. Results are similar for islands of other sizes in the range of possibilities under consideration.

The increment of energy per Pt atom upon detachment, however, does not depend significantly on the island size, but varies within the range of 0.11–0.14 eV. For instance, for a two-atom Pt island, detachment leads to an increase in E_{form} from -10.46 to -10.24 eV while, for a three-atom island, the energy increases from -15.88 to -15.56 eV upon detachment. We thus obtain a clear trend: the larger the two-dimensional

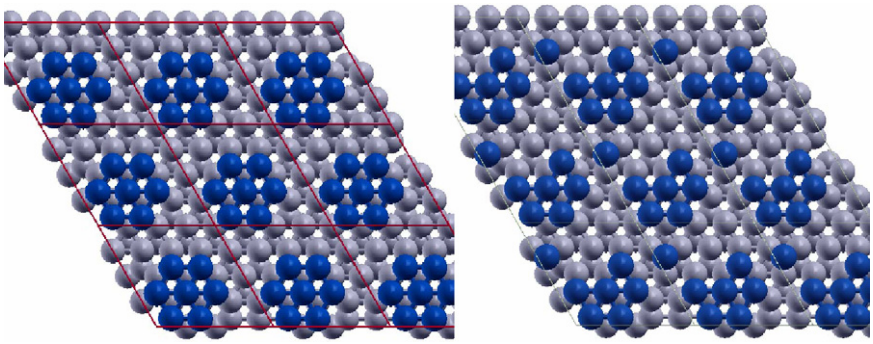

Figure 3. Two configurations of a seven-atom Pt island (dark (or blue in the online version) balls) on Ru(0001) (light (or gray in the online version) balls) showing the detachment of one Pt atom.

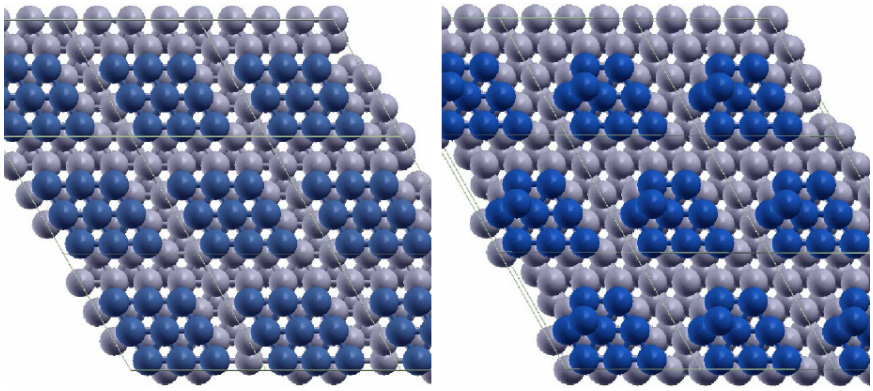

Figure 4. Two configurations of a nine-atom Pt island (dark (or blue in the online version) balls) with 2D (left) and 3D (right) structures on Ru(0001) (light (or gray in the online version) balls).

Pt island (up to 1 ML), the lower its formation energy per atom is. Thus, assuming that the free energy of the system in consideration is dominated by its DFT total energy, we conclude that Pt tends to wet Ru(0001).

We have also performed calculations for some 3D Pt configurations on Ru(0001) and found that their 2D isomers have lower energy. For example, two configurations of a nine-atom Pt island with 2D and 3D structures (see figure 4) were found to have $E_{\text{form}} = -50.06$ eV and -48.54 eV, respectively.

The above results indicate the propensity of Pt atoms to increase their local coordination and thus form 2D islands up to full coverage when adsorbed on Ru(0001)—and that this propensity is strong enough to overpower the stress effects derived from the Pt–Ru bond-length misfit. This preponderance holds only at low temperatures and after a long relaxation time. As mentioned above, to take into account the kinetics of the system, we have also looked at the diffusivity of a Pt ad-atom in the event that it is adsorbed on top of Pt islands. The question is thus whether the Pt ad-atom will be trapped on top of the Pt island (as shown in the right inside of figure 4) or will descend at the kink site on the Ru(0001) surface (left inside of figure 4). Our calculated activation barrier of the Pt monomer diffusion on the eight-atom Pt island from hcp to fcc is 0.23 eV and from fcc to hcp is 0.09 eV. The activation barrier for the descendant step of a Pt monomer from fcc to the kink site on the Ru(0001) is 0.39 eV (and 1.92 eV for the inverse process). We thus obtain the Schwoebel barrier of the heteroepitaxial descendant step of Pt to be +0.30 eV. Since it is positive, it points to 3D clustering growth. However, a word of caution must be inserted here. The Ru nanoparticles that we are trying to understand are decorated with Pt at very low coverage (∼0.1 ML) through spontaneous deposition via a $[PtCl_6]^{2-} + 0.1$ M Hi_2SO_4 solution [6]. With such a technique, the probability of a Pt ad-atom to fall on top of the island is low. Besides, there is an indication [64] that, even in the case of positive Schwoebel barriers, as long as the atom deposition rate is low and the diffusion speed fast, the reflective property of steps is valid only at temperatures well below room temperature for fcc(111) metals. In that regard, it is worth mentioning that, as reported [65], at low coverage of 0.03 ML of Pt, 2D islands (of ∼2 nm) are formed on Ru(0001) and, furthermore, the 2D/3D crossover depends on experimental conditions.

There still remains the question: why, despite the misfit, are 2D configurations favorable? In order to grasp some understanding of the issue, we note first that, in the 2D Pt islands under consideration, the number of NN varies from 3 (single atom) to 9 (full monolayer). Decrease in the number of NN usually causes reduction of the equilibrium interatomic distances. Indeed, we find that, for a free-standing Pt monolayer, in which every Pt atom has only six nearest neighbors, the equilibrium Pt–Pt NN distance is much shorter (∼2.6 Å) than that in bulk Pt (∼2.8 Å) and even shorter than

the Ru–Ru NN distance in bulk Ru (∼2.71 Å). The misfit in low-dimensional structures is thus not a well-defined quantity because of its dependence on the coordination number of the atoms in question. For these surface alloys, there is also the issue of stress induced by the bond-length misfit between the Pt nanostructures and the Ru surface atoms, neither one of which is expected to be at the bulk value, given the diversity of their local geometric environment. For the Pt atoms on the top of an hcp metal such as Ru, there is also incommensurability in bulk structure. We find that the bulk NN bond length of Pt atoms certainly decreases when they arrange on an hcp structure. In that case, the bulk bond-length misfit between Pt and Ru decreases from 2.8% to 1.4%. Furthermore, the surface interlayer distance in Pt(111) expands to 2.49 Å (1.0% with respect to bulk), while that of the hypothetical Pt(0001) contracts to 2.39 Å notwithstanding that intralayer NN distances are 1.8% smaller than in the fcc bulk.

3.2. Modeling Pt diffusion through the edges of Ru nanostructures

From the above, we have gained an understanding of the tendency of Pt atoms to form a 2D layer—wetting the Ru(0001) surface—rather than clustering in multiple 2D or 3D structures.

In this case, however, even for low coverage (∼0.1 ML), a large island should completely cover one of the facets of the Ru nanoparticles. For example, for the Ru nanoparticle of 2.5 nm with the proposed cubo-octahedral structure [7], the 0.1 ML of Pt coalesced into a single island would fully cover one of the squared facets, while experiments suggest that Pt islands maintain a 5- to 7-atom size on Ru nanoparticles for such coverage [7]. To resolve this discrepancy we need to note that one main difference between the infinite Ru(0001) surface and the Ru nanoparticle is that the latter exhibits edges dividing its facets. These edges may be obstacles for Pt atom diffusion. If this is true, 2D islands formed on each facet do not join together into a large single island because the edges prevent those initial small islands from diffusing to other facets, enabling them to persist as few-atom 2D islands.

To check this hypothesis, we simulate two kinds of edges of the Ru nanoparticle and calculate diffusion barriers of Pt monomers and dimers through these edges. We model the diffusion through the edges formed by facets of (0001) and (1101) geometry, which are among the most stable Ru surfaces [7, 66]. The supercell in this case contains 116 Ru atoms with a four-atom wide Ru(0001) facet and two Ru(1101) facets (see figure 5). The construction of this Ru supercell, which has 7 × 4 in-plane periodicity, is achieved by stacking five Ru(0001) layers: two of 7 × 4, one of 6 × 4, one of 5 × 4 and one of 4 × 4 atoms. The edges thus obtained on each side of the Ru(0001) have different local geometries, which for convenience are labeled as A and B. Atoms forming edge A (edge B) are contiguous to hcp (fcc) hollow sites of the (0001) facet. The bottom two layers (see figure 5) were not allowed to relax to guarantee the stability of the superstructure. We impose a 15 Å vacuum layer between periodic superstructures along the direction perpendicular to the surface, as in the system described previously. The Brillouin zone is sampled with a (2 × 3 × 1) *k*-point mesh. The adsorption energy and diffusion barriers of Pt monomers and dimers are calculated on the (0001) and (1101) facets.

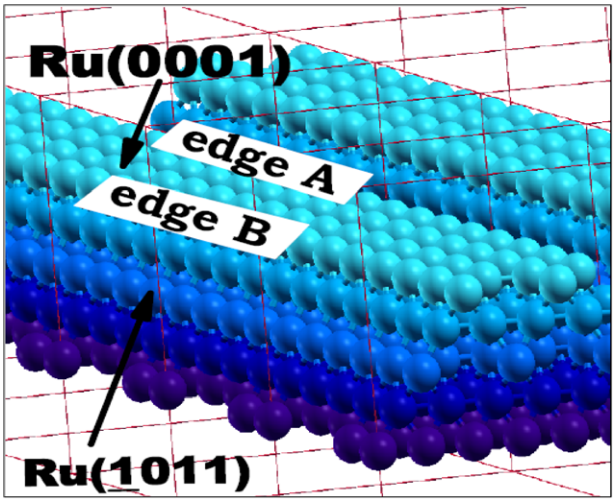

Figure 5. Model of the edges of a faceted Ru nanoparticle exposing a (0001) facet and two (1101) facets. Different tones of gray (blue) distinguish the five layers parallel to the (0001) surface constituting the structure.

3.2.1. Pt monomers. The structure shown in figure 5 possesses 3 hcp and 3 fcc non-equivalent hollow sites on the (0001) facet. The adsorption energy of a Pt monomer calculated for all these sites is within the −4.77 to −5.05 eV range. We find that for all hcp sites E_{ad} is higher (absolute value is lower, binding is weaker) than for any fcc site. In addition, Pt monomers preferably reside on sites surrounded by 2-edge atoms, rather than on those surrounded by only a 1- or 0-edge atom. Across edge A, the first (1101) available site is a fourfold hollow site whose adsorption energy, −5.66 eV, is substantially lower than that on hcp sites of the (0001) facet. Across edge B, the first (1101) available site is a threefold hollow site, whose adsorption energy is −4.92 eV.

The calculated diffusion barrier ΔE of the monomer through edge A is found to be highly asymmetric. It is equal to 0.49 eV for diffusion from fcc site 1 on (0001) to the nearest site in the (1101) facet, but 1.10 eV to diffuse back. Applying equation (1) we obtain the rate for the (0001) → (1101) diffusion at room temperature to be 6×10^3 s^{-1}, which is much lower than that for the diffusion on the facet. The back diffusion rate, however, appears to be negligibly low.

The shortest path for diffusion through edge B connects the hcp site on the (0001) facet with the threefold hollow site on the (1101) facet. The barrier for diffusion along this path is found to be 0.28 eV, which is just slightly higher than the barriers for diffusion on the facet. However, the initial state for this process (hcp site) is not an equilibrium state. Its total energy is 0.08 eV higher than that for the monomer adsorbed on the neighboring fcc site. It thus makes sense to consider the diffusion of the Pt monomer through edge B as a two-step process with diffusion from the fcc to the hcp site on (0001) and then from that to the threefold site on (1101).

This substantially reduces the overall probability of diffusion through edge B. Moreover, the fact that the fcc–hcp barrier is asymmetric (0.20 eV for fcc → hcp, but 0.12 eV to diffuse back) further reduces the diffusion probability. Our results thus suggest that the considered edges are significant obstacles for diffusion of Pt atoms, and thus possible factors inhibiting formation of large Pt islands on the Ru nanoparticles.

3.2.2. Pt dimers. The results of the previous section (3.2.1) suggest that the low diffusion rate of the Pt monomers through the edge between the facets is a factor controlling the size of the Pt islands on the Ru nanoparticles. Since the result for the monomer diffusion through edge B is not so tractable, we also consider the diffusion of the Pt dimer through that edge.

First, we find E_{form}/n to be higher by 0.12 eV for the dimer than for the monomer, suggesting that dimers would preferably form rather than diffuse as two monomers through the easy edges. As in the case of monomers, dimers prefer to sit on hcp sites on the (0001) facet. On the (0001) facet, when one of the atoms in the dimer comes closer to the edge and its coordination is reduced from 5 to 4, E_{form}/n drops by 0.16 eV, suggesting that there is a higher barrier for Pt dimers to approach the edges to the point where its atoms become more undercoordinated.

Figure 6 illustrates the calculated path and energetic for the diffusion of the dimer across edge B. As seen from the figure, this is a complex process, which comprises two stages with an intermediate energy minimum in which one Pt atom is on the fcc site closest to the edge of (0001), while the other is on the threefold site in (1101). Given the comparatively high barriers, the diffusion rates for the successive steps are estimated to be three orders of magnitude lower than those of the monomer, suggesting that the probability for the Pt dimer to perform the two-step diffusion through edge B is negligible. As a result of the complex geometric structure of the edge, there could be no diffusion path for the Pt dimer between the facets without significant change of the Pt–Pt and Pt–Ru bond lengths. Such changes increase the total energy of the system and thus result in a high diffusion barrier. A simple geometrical analysis suggests that, in the case of trimer or larger islands, these effects are even more pronounced and the rates of their diffusion through the edges will diminish.

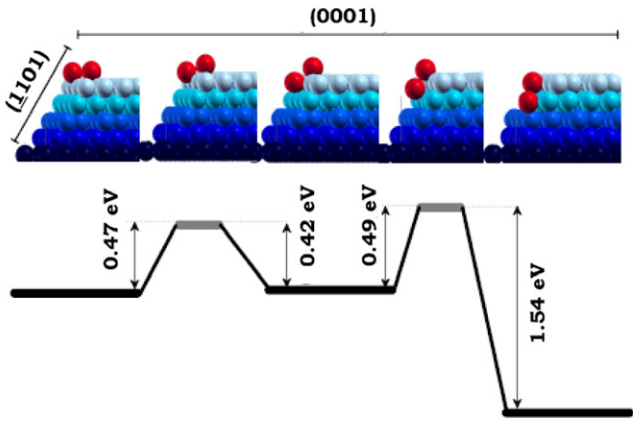

Figure 6. The upper five panels from left to right illustrate the two-step diffusion of the dimer (red) across the edge intersecting the (0001) and the (1101) facets (blue). First, third, and fifth upper panels are local minimum energy configurations of the dimer and the second and fourth upper panels are the transition states. The lower panel shows the energetics for diffusion of the dimer between the (0001) and (1101) facets.

4. Summary

As an example of the application of DFT-based methods for understanding the microscopic processes that control the characteristics of fuel cell catalysts, we have presented here a review of recent results which provide a rationale for the observed high CO tolerance of the electrocatalyst based on the Ru nanoparticles with sub-monolayer Pt coverage. We find the energetics of CO adsorbed on the system to be such that CO tends to diffuse from catalytically active Pt onto the Ru substrate. This mechanism requires Pt islands to be small (consisting of only a few atoms). Meanwhile our further calculations show the propensity of Pt atoms to coalesce and form as large an island as possible. This is, however, true for the flat Ru(0001) surface, while the Ru nanoparticles of interest exhibited a number of flat facets divided by edges. We find that diffusion of Pt atoms and dimers through the edges between Ru facets is prevented by high activation energy barriers. This finding reveals why the nanosize of Ru particles is so critical. Pt atoms adsorbed on a particle of such a size with sub-monolayer coverage do not move from one facet to the other through the edges, but rather form small islands on the facets they were adsorbed on. This result in the configuration is favorable for CO spillover from the active Pt sites, which reduces CO poisoning of this catalyst. The literature, of course, is abundant with other examples that show the power of DFT as a reliable tool in computational design of fuel cell catalysts.

Acknowledgments

We thank Radislav Adzic for bringing this subject to our attention and for fruitful discussions. We are grateful to Lyman Baker for a critical reading of the manuscript. The work was supported in part by DOE under grant no. DE-FG02-07ER15842 and DE-FG02-07ER46354.

References

[1] Basic research needs for hydrogen economy *Report of BES Workshop (May, 2003)* http://www.sc.doe.gov/bes/reports/files/NHE_rpt.pdf
[2] Ralph T R and Hogarth M P 2002 *Platinum Met. Rev.* **46** 117
[3] Vielstich W, Lamm A and Gasteiger H A (ed) 2003 *Handbook of Fuel Cells: Fundamentals, Technology, and Applications* (Chichester: Wiley)
[4] Cruickshank J and Scott K 1998 *J. Power Sources* **70** 40
[5] Samjeské G, Wang H, Löffler T and Baltruschat H 2002 *Electrochim. Acta* **47** 3681
[6] Brankovic S R, Wang J X and Adžic R R 2001 *Electrochem. Solid State Lett.* **4** A217
[7] Brankovic S R, Wang J X, Zhu Y, Sabatini R, McBreen J and Adžic R R 2002 *J. Electroanal. Chem.* **524/525** 231
[8] Mukerjee S and Srinivasan S 1993 *J. Electroanal. Chem.* **357** 201

[9] Stamenkovic V R, Mun B S, Arenz M, Mayrhoffer K J J, Lucas C A, Wang G, Ross P N and Markovic N M 2007 *Nat. Mater.* **6** 241
[10] Zhang J, Vukmirovic M B, Xu Y, Mavrikakis M and Adzic R R 2005 *Angew. Chem. Int. Edn* **44** 2132
[11] Wang W, Zheng D, Du C, Zou Z, Zhang X, Xia B, Yang H and Akins D L 2007 *J. Power Sources* **167** 243
[12] Adzic R R, Zhang J, Sasaki K, Vukmirovic M B, Shao M, Wang J X, Nilekar A U, Mavrikakis M, Valerio J A and Uribe F 2007 Platinum monolayer fuel cell electrocatalysts *Top. Catal.* **46** 249
[13] Nilekar A and Mavrikakis M 2008 Improved oxygen reduction reactivity of platinum monolayers on transition metal surfaces *Surf. Sci.* **602** L89
[14] Mustain W E, Kepler K and Prakash J 2006 *Electrochim. Commun.* **8** 406
[15] Mustain W E, Kepler K and Prakash J 2007 *Electrochim. Acta* **52** 2102
[16] Liu H and Manthiram A 2009 *Energy Environ. Sci.* **2** 124
[17] Lee K, Zhang L and Zhang J 2007 *J. Power Sources* **170** 291
[18] Zhong H, Zhang H, Liu G, Liang Y, Hu J and Yi B 2006 *Electrochem. Commun.* **8** 707
[19] Chen Y G, Zhuang L and Lu J T 2007 *Chin. Chem. Lett.* **18** 1301
[20] Xiao L, Zhuang L, Liu Y, Lu J and Abruña H D 2009 *J. Am. Chem. Soc.* **131** 602
[21] Xia D, Liu S, Wang Z, Chen G, Zhang L, Zhang L, Hui S and Zhang J 2008 *J. Power Sources* **177** 296
[22] Zhong H, Chen X, Zhang H, Wang M and Mao S S 2007 *Appl. Phys. Lett.* **91** 163103
[23] Kim J-H, Ishihara A, Mitsushima S, Kamiya N and Ota K 2007 *Chem. Lett.* **36** 514
[24] Bezerra C W B, Zhang L, Lee K C, Liu H S, Marques A L B, Marques E P, Wang H J and Zhang J J 2008 *Electrochim. Acta* **53** 4937
[25] Yang R, Bonakdarpour A, Easton E B, Stoffyn-Egli P and Dahn J R 2007 *J. Electrochem. Soc.* **154** A275
[26] Yang R, Dahn T R, Dahn H M and Dahn J R 2008 *J. Electrochem. Soc.* **155** B327
[27] Ohgi Y, Ishihara A, Shibata Y, Mitsushima S and Ota K 2008 *Chem. Lett.* **37** 608
[28] Ishihara A, Lee K, Doi S, Mitsushima S, Kamiya N, Hara M, Domen K, Fukuda K and Ota K 2005 *Electrochem. Solid-State Lett.* **8** A201
[29] Gambardella P *et al* 2001 *Phys. Rev. Lett.* **87** 056103
[30] Hohenberg P and Kohn W 1964 *Phys. Rev.* **136** B864
[31] Kohn W and Sham L J 1965 *Phys. Rev.* **140** A1133
[32] Groß A 2002 *Surf. Sci.* **500** 347 and references herein
[33] Reuter K, Frenkel D and Scheffler M 2004 *Phys. Rev. Lett.* **93** 116105
[34] Nørskov J K, Rossmeisl J, Logadottir A, Lindqvist L, Kitchin J R, Bligaard T and Jonsson H 2004 *J. Phys. Chem.* B **108** 17886
[35] Anderson A B and Albu T V 1999 *Electrochem. Commun.* **1** 203
[36] Anderson A B and Albu T V 1999 *J. Am. Chem. Soc.* **121** 11855
[37] Shi Z, Zhang J, Liu Z-S, Wang H and Wilkinson D P 2006 *Electrochem. Acta* **51** 1905
[38] Karlberg G S, Rossmeisl J and Nørskov J K 2007 *Phys. Chem. Chem. Phys.* **9** 5158
[39] Filhol J-S and Neurock M 2006 *Angew. Chem. Int. Edn* **45** 402
Taylor C D, Wasileski S A, Filhol J-S and Neurock M 2006 *Phys. Rev.* B **73** 165402
[40] Rossmeisl J, Nørskov J K, Taylor C D, Janik M J and Neurock M 2006 *J. Phys. Chem.* B **110** 21833
[41] Stolbov S, Alcántara Ortigoza M, Rahman T S and Adzic R 2009 *J. Chem. Phys.* **130** 124714
Alcántara Ortigoza M, Stolbov S and Rahman T S 2008 *Phys. Rev.* B **78** 195417
[42] Koper M T, Shubina T E and van Santen R A 2002 *J. Phys. Chem.* B **106** 686
[43] Tsuda M and Kasai H 2006 *Phys. Rev.* B **73** 155405
[44] Schlapka A, Lischka M, Groß A, Käsberger U and Jakob P 2003 *Phys. Rev. Lett.* **91** 016101
[45] Sasaki K, Wang J X, Balasubramanian M, McBreen J, Urbe F and Adžic R R 2004 *Electrochim. Acta* **49** 3873
[46] Payne M C, Teter M P, Allan D C, Arias T A and Joannopoulos J D 1992 *Rev. Mod. Phys.* **64** 1045
[47] Kresse G and Furthmuller J 1996 *Phys. Rev.* B **54** 11169
[48] Vanderbilt D 1990 *Phys. Rev.* B **41** 7892
[49] Monkhorst H J and Pack J P 1976 *Phys. Rev.* B **13** 5188
[50] Perdew J P and Wang Y 1992 *Phys. Rev.* B **45** 13244
[51] Feibelman P J, Hammer B, Norskov J K, Wagner F, Scheffler M, Stumpf R, Watwe R and Dumesic J 2001 *J. Phys. Chem.* B **105** 4018
[52] Mavrikakis M, Rempel J, Greeley J, Hansen L B and Nørskov J K 2002 *J. Chem. Phys.* B **117** 6737
[53] Grinberg I, Yourdshahyan Y and Rappe A M 2002 *J. Chem. Phys.* B **117** 2264
[54] Kresse G, Gil A and Sautet P 2003 *Phys. Rev.* B **68** 073401
[55] Markov I V 2003 *Crystal Growth for Beginners* (Singapore: World Scientific)
[56] Chang T M and Carter E A 1995 *J. Phys. Chem.* **99** 7637
[57] Copel M, Reuter M C, Kaxiras E and Tromp R M 1989 *Phys. Rev. Lett.* **63** 632
[58] Shuttleworth R 1949 *Proc. Phys. Soc.* A **62** 167
[59] Kumikov V K and Khokonov K B 1982 *J. Appl. Phys.* **54** 1346
[60] Kittel C 1976 *Introduction to Solid State Physics* (New York: Wiley)
[61] Tersoff J 1995 *Phys. Rev. Lett.* **74** 434
[62] Schwoebel R L 1969 *J. Appl. Phys.* **40** 614
[63] Tsong T T and Fu T Y 1997 *Appl. Surf. Sci.* **121/122** 34
[64] Tsong T T 2003 *Prog. Surf. Sci.* **74** 69
[65] Hoster H, Richter B and Behm R J 2004 *J. Phys. Chem.* B **108** 14780
[66] Morrow P, Tang F, Karaback T, Wang P I, Ye D X, Wang G C and Lu T M 2006 *J. Vac. Sci. Technol.* A **24** 237